Reproducible nucleation and control of stable quantum vortex rings in Bose-Einstein condensates

Letter

Reproducible nucleation and control of stable quantum vortex rings in Bose-Einstein condensates

Giorgia Iori [1], Klejdja Xhani [2], Woo Jin Kwon [1,3], Davide Emilio Galli [1,*], and Luca Galantucci [4,5,†]

[1]*Dipartimento di Fisica "Aldo Pontremoli", Università degli Studi di Milano, via Celoria 16, I-20133 Milano, Italy*

[2]*Dipartimento Scienza Applicata e Tecnologia, DISAT, Politecnico di Torino, I-10129 Torino, Italy*

[3]*Department of Physics, Ulsan National Institute of Science and Technology (UNIST), 44919 Ulsan, Republic of Korea*

[4]*Istituto per le Applicazioni del Calcolo, Consiglio Nazionale delle Ricerche, via dei Taurini 19, I-00185 Roma, Italy*

[5]*School of Mathematics, Statistics and Physics, Newcastle University, Newcastle upon Tyne NE1 7RU, United Kingdom*

(Received 13 March 2026; accepted 11 May 2026; published 5 June 2026)

We propose and numerically validate an experimentally feasible on-demand protocol for the nucleation and manipulation of stable quantum vortex rings in trapped Bose-Einstein condensates. The method relies on sweeping a laser-sheet barrier that locally constricts the superflow and triggers vortex-ring formation. By tuning the barrier height and width, and by scanning the barrier velocity, we identify the onset of periodic generation of vortex rings above the critical velocity and achieve direct, deterministic control over the ring nucleation position, radius, and hence propagation speed. After its formation, *ad hoc* optical potentials are applied to reshape the vortex ring, creating clean Kelvin-wave excitations. Our results provide a foundation for systematic studies of three-dimensional vortices in atomic superfluids and open the door to tailored vortex dynamics and interactions, enabling controlled access to quantum turbulence.

DOI: 10.1103/qvg7-mr18

Introduction. Coherent filamentary structures are ubiquitous across physical systems, from classical fluids and plasmas to optical fields and quantum matter. Their dynamics play a key role in determining the macroscopic properties of nematic liquid crystals [1], plasmas (from astrophysical flows [2–4] to nuclear fusion devices), and optical beams [5,6], as well as classical [7,8] and quantum fluids [9–11].

In fluid systems, these coherent structures correspond to vortices: localized regions of concentrated vorticity that organize the surrounding flow and play a central role in turbulence. Through nonlinear interactions and vortex stretching, vortices drive the turbulent cascade [12], redistributing kinetic energy across length scales according to the Kolmogorov spectrum [13], observed in both classical and quantum turbulent flows [14–17]. At the smallest scales, vortices are ultimately responsible for energy dissipation, either through viscosity in classical fluids or via mutual friction [18] and Kelvin-wave cascades [18–22] in quantum fluids.

The nature of vortices is fundamentally dictated by whether the fluid is classical or quantum. In classical fluids, vortices are unconstrained in strength, size, and geometry and are dissipated by viscosity. In contrast, in quantum fluids—such as superfluid helium [11], ultracold atomic gases [23], polariton condensates [24], and the interior of neutron stars [25]—vorticity is confined to discrete, effectively one-dimensional vortex lines with quantized circulation and fixed core size [26–28]. These vortex lines are topological defects of the order parameter and constitute stable excitations in homogeneous quantum fluids at zero temperature. Their discrete filamentary nature, together with the exceptional experimental tunability of Bose-Einstein condensates (BECs), makes ultracold gases an ideal platform for investigating fundamental vortex dynamics, including vortex reconnections [29–31], vortex-boundary interactions [32], and Kelvin-wave excitations [33]. The relevance of these studies goes beyond quantum fluids as, due to striking observed similarities between quantum and classical turbulence [14,34–36], the suggestive idea that turbulent flows, both classical and quantum, may be described in terms of the mutually interacting dynamics of discrete and thin vortex filaments of fixed circulation has been put forward [37,38].

Despite this progress, a central experimental challenge is the on-demand, reproducible generation of individual three-dimensional (3D) quantum vortices, with control over their geometry, dynamics, and lifetime. While in two dimensions the topic has been successfully tackled in both Bose and Fermi atomic superfluids employing the so-called chopstick method [39,40], in three dimensions, this remains challenging because additional degrees of freedom (e.g., Kelvin-wave excitations) can reduce vortex lifetime and affect stability. In 3D condensates, vortices are currently generated either stochastically via the Kibble-Zurek mechanism [41], through Josephson junction dynamics [42], or by driving the condensate with quantum pistons [43]. In all these approaches, the absence of precise control over vortex number, geometry, and reproducibility hinders systematic studies of vortex interactions. Numerical studies have provided relevant insight into 3D

*Contact author: davide.galli@unimi.it

†Contact author: luca.galantucci@cnr.it

vortex nucleation in trapped condensates [44–47] in the context of the critical velocity determination, vortex-ring dynamics, and classification of generated solitary waves (vortex rings or rarefaction pulses [48]), related to small and unstable vortex rings (radii smaller than five times the coherence length). Nevertheless, many aspects of the direct control of stable vortex rings remain elusive.

In this work, we numerically demonstrate a protocol for the controlled nucleation and manipulation of stable and reproducible quantum vortex rings in trapped Bose-Einstein condensates. By employing a moving laser sheet, we achieve precise control over the nucleation position, size, shape, and propagation velocity of vortex rings, as well as their number and generation frequency. Breaking the axial density symmetry by applying localized beams in the downstream, we further enable controlled excitation of Kelvin waves, paving the way for systematic studies of quantum vortex excitations.

Problem and approach. We model the dynamics of trapped Bose-Einstein condensates employing the mean-field Gross-Pitaevskii framework [49] according to which the order parameter $\Psi(\mathbf{x}, t)$ of the system is governed by the following equation:

$$i\hbar\frac{\partial\Psi}{\partial t} = -\frac{\hbar^2}{2m}\nabla^2\Psi + g|\Psi|^2\Psi + V\Psi - \mu\Psi\ , \qquad (1)$$

where m is the mass of boson considered, $g = 4\pi\hbar^2 a_s/m$ is the two-body interaction strength, a_s being the s-scattering length, $V = V(\mathbf{x}, t)$ is the externally applied potential, and μ is the chemical potential, related to the number of particles N and a_s via the normalization condition $\int|\Psi|^2 d\mathbf{x} = N$. The potential $V = V_h + V_b$ is composed of the static cylindrical harmonic potential $V_h(\mathbf{x}) = \frac{1}{2}m\omega_\perp(x^2 + y^2)$, where $\omega_\perp = 2\pi\,150\,\mathrm{Hz}$ is the radial trapping frequency, and the time-dependent planar barrier potential $V_b(\mathbf{x}, t) = V_b(z, t) = V_0 e^{-\frac{(z-z_b(t))^2}{2\sigma_b^2}}$, where V_0 is the tunable barrier intensity, σ_b is the width of the barrier, and $z_b(t)$ is the controllable position of the center of the barrier. The potential V_b describes the impact on the condensate of the axial sweep of a laser sheet of width σ_b. In our study, the barrier moves with a gradually ramped-up time velocity $v_b(t) = v_b^{\max}\tanh(t/\tau_b)$ [50] from an initial axial position z_0. We choose a cylindrical condensate, with no axial trapping ($\omega_z = 0$), in order to study in an idealized setting the dynamics occurring in the central region of an experimentally realizable cigar-shaped condensate. The radial size of the condensate far from the barrier is $R_{\perp_\infty} = \sqrt{2\mu/(m\omega_\perp^2)}$ in the limit of large N, which we satisfy as we choose $N \sim 1.5\times10^5$ pairs of ^{6}Li atoms, implying thus $m = 2\times10^{-26}\,\mathrm{kg}$ and $a_s = 5.3\times10^{-8}\,\mathrm{m}$. Details on the numerical simulations are reported in the Supplemental Material [50] and hereafter all quantities will be indicated in dimensionless units, the units of length, time, and energy being, respectively, $\ell_\perp = \sqrt{\hbar/(m\omega_\perp)}$, $\tau_\perp = \omega_\perp^{-1}$, and $\epsilon_\perp = \hbar\omega_\perp$ [53].

The vortex nucleation process is as follows. At time $t = 0$, we start moving the barrier toward the positive z direction from the initial position $z_0 = -R_{\perp_\infty}$, which we choose arbitrarily without loss of generality. The motion of the barrier is equivalent (with a Galileian transformation) to forcing the fluid (the condensate) to flow in a constricted geometry, accelerating its speed. In fact, the presence of the moving barrier narrows the radial size of the condensate, which at $z = z_b(t)$ is equal to $R_{\perp_b} = \sqrt{2(\mu - V_0)} < R_{\perp_\infty} = \sqrt{2\mu}$ (in nondimensional units), and depletes the particle density n of the condensate $n_b(r) = n(r, z)|_{z=z_b(t)} = (\mu - V_0 - V_h(r))/C < (\mu - V_h(r))/C = n_\infty(r)$, where r is the radial coordinate, $C = 4\pi N a_s/\ell_\perp$ is the nondimensional interaction strength [50], and $n_\infty(r)$ is the radial density profile far from the barrier. The conservation of the mass flux thus implies that at the barrier, the average axial relative velocity $\bar{v}_b^z$ between the condensate and the barrier is larger than the average relative velocity $\bar{v}_\infty^z$ far from the barrier itself, and as we move radially toward the boundaries of the condensate the axial velocity increases, due to the presence of quantum pressure effects [44]. Therefore, the maximum relative velocity between the barrier and the condensate occurs at $z = z_b(t)$ near the boundary ($r \sim R_{\perp_b}$). Density depletion there lowers the local sound speed c, closely related to the critical velocity for vortex nucleation either via the Landau criterion ($v_c = c$) [54–56] or via the triggering of a transonic transition determined by the change of the nature of the differential equation governing the flow (elliptic to hyperbolic [57–59]). Exceeding this critical velocity causes the nucleation of a vortex ring at the barrier edge, as shown in Fig. 1 (left).

As the tunable barrier intensity V_0 is increased, the constriction of the flow is more pronounced, leading to a narrower flow cross section and thus to a stronger acceleration of the flow at the barrier. Hence, a smaller velocity of the barrier is needed in order to exceed the local critical velocity and nucleate the first vortex ring. We indicate the smallest velocity of the barrier $v_b^{\max}$ at which we observe vortex nucleation as the critical velocity v_c and report its behavior as a function of V_0/μ in the main panel of Fig. 2, showing indeed a decrease of v_c for increasing V_0. A similar behavior of v_c is observed experimentally in two dimensions [56]. We also study the variation of v_c for increasing barrier width σ_b (Fig. 2, main panel; top axis), observing that the critical velocity reaches a plateau once the width has reached the size of a vortex core $a_0 \sim 5\xi$, $\xi = 1/\sqrt{2\mu}$ being the healing length on the trap axis, as observed in homogeneous condensates [55,60].

Once nucleated, the vortex undergoes a dynamics whose main stages are reported in Fig. 1, with three-dimensional renderings (top row) and two-dimensional density and phase plots on the horizontal $y = 0$ plane (bottom row); vortices are tracked with an algorithm based on the pseudovorticity [61,62] (top) and identified by density depletions and phase defects (bottom). We observe indeed the nucleation of a vortex ring near the boundary in the barrier region (Fig. 1, left panel). Its nucleation corresponds to an injection of energy (mainly kinetic) into the condensate resulting from the work performed by the barrier on the condensate itself (see Appendix B). The nucleation process, in fact, strongly breaks the upstream-downstream density symmetry at the barrier, generating a force performing the work and injecting the energy into the condensate. The dynamics of the vortex ring instead is driven by its self-induced velocity, while its shrinking arises from density gradient forces or, equivalently, from energy conservation constraints (Fig. 1, central panel). Far from the barrier, the ring propagates at a constant velocity, preserving its shape (Fig. 1, right panel).

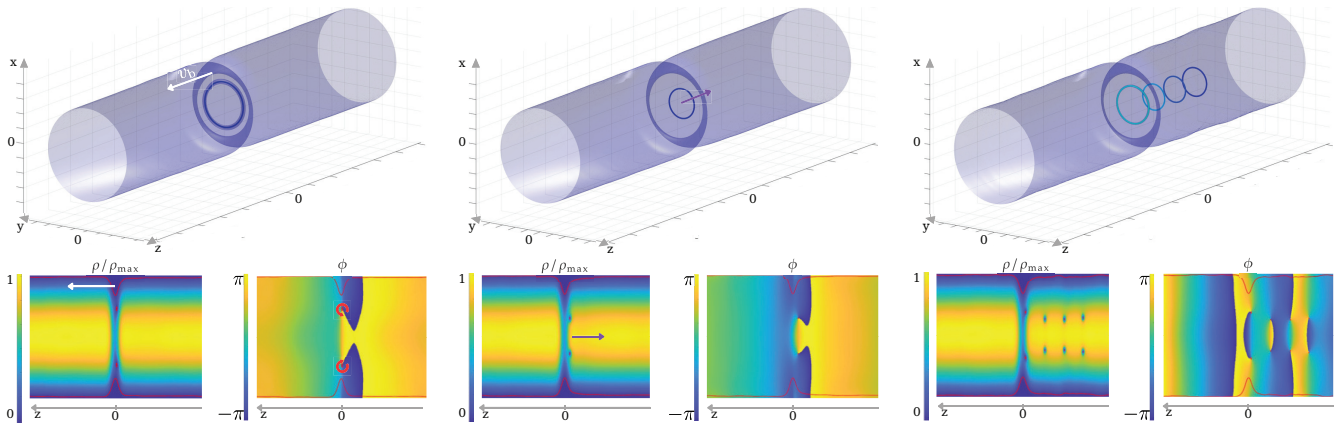

FIG. 1. Stages of vortex ring nucleation and evolution, shown via BEC density isosurfaces at 5% of the maximum density and density ρ-phase ϕ projections on the plane $y = 0$ at different times in the reference frame where the barrier is stationary. Left panel: Ring generation triggered by the moving barrier (white arrow); red arrows in the phase snapshot indicate the circulation of the velocity field. Central panel: Shrinking across the barrier: the ring propagates opposite to the barrier motion (purple arrow), while its radius decreases. Right panel: Propagation in the bulk and periodic generation: the first ring reaches an asymptotic regime with constant radius and velocity; meanwhile, additional rings are generated periodically and eventually reach the same asymptotic properties. In the isosurfaces, the vortex rings are represented by circles displayed in different shades of blue. The red curves on the density-phase plots show the low-density isocontour at 2.5% of the maximum density, marking the condensate edge and the density depletions corresponding to vortex cores.

It is worth noting that the nucleated vortex ring travels opposite to the barrier motion, unlike the vortices generated by the flow around a single obstacle (e.g., a disk in two dimensions) [63,64]. Instead, its propagation direction coincides with that of vortices generated between multiple obstacles [65].

Once $v_b \gtrsim v_c$, we observe periodic generation of vortex rings, each undergoing the same dynamical evolution [Fig. 1 (right)], the frequency of nucleation increasing approximately linearly with the barrier velocity, as reported in the inset of Fig. 2. When the frequency is sufficiently large [empty symbols in Fig. 2 (inset)], the distance between vortices is small enough to trigger a leapfrogging dynamics [47,66].

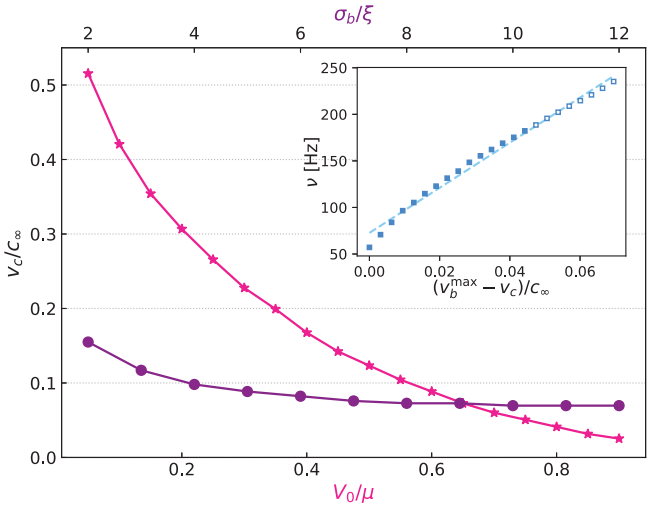

FIG. 2. Critical velocity v_c for vortex ring nucleation as a function of barrier height V_0/μ (pink stars, fixed $\sigma_b = 5\xi$) and of barrier width σ_b (purple circles, fixed $V_0 = 0.6\,\mu$). Inset: vortex nucleation frequency ν at fixed $V_0 = 0.6\,\mu$ and $\sigma_b = 5\xi$ as a function of barrier velocity $v_b^{\max} > v_c$ (blue squares), spanning from v_c to $1.78v_c$; the dashed line represents a linear fit of the data. Empty squares represent the cases where we observe leapfrogging events. Velocities are expressed in units of the density-averaged speed of sound $c_\infty = \sqrt{\mu/2}$.

In order to study reproducibly vortex interactions, it is essential to be able to predict the size of the generated vortex rings. In Fig. 3 (top), we report the initial (light blue) and asymptotic (lilac) radii R of the generated vortex rings as a function of V_0/μ and their behavior as we vary the barrier width σ_b for $V_0/\mu = 0.6$ (inset). The initial radius clearly follows the radial width of the condensate at the barrier $R_{\perp_b}$ indicated with a dashed curve in Fig. 3 (top). The difference between initial and asymptotic values increases with V_0/μ: Indeed larger V_0 implies larger density gradients, which are responsible for the shrinking of the vortex ring. The inset of Fig. 3 (top) shows again that the width of the barrier σ_b only impacts when smaller than a_0.

The other key element to investigate vortex interactions deterministically is the vortex ring velocity. While in a homogeneous and unbounded condensate the expression relating radius R and velocity V^z is straightforward, namely, $V^z \sim 1/R$ for R sufficiently larger than ξ [67], the existence of boundaries [68] and/or the presence of inhomogeneous density backgrounds [69,70] introduce additional physical effects whose nonlinear combination governs the speed and the direction of the generated vortex ring. The density depletion near the boundary of a condensate indeed shifts the position of the image vortex [68], which together with the density gradient dictates the velocity of the vortex ring. The measured asymptotic velocity of the nucleated rings is reported in Fig. 3 (bottom) as a function of the ring radius R. Three nontrivial characteristics emerge clearly: First, there is a direction inversion of the ring's motion; second, this change of velocity sign does not occur at $R/\xi = 20$ ($R/R_{\perp_\infty} = 0.5$); and third, the velocity magnitude is not symmetrical with respect to $V^z = 0$. The change of direction of the vortex ring motion

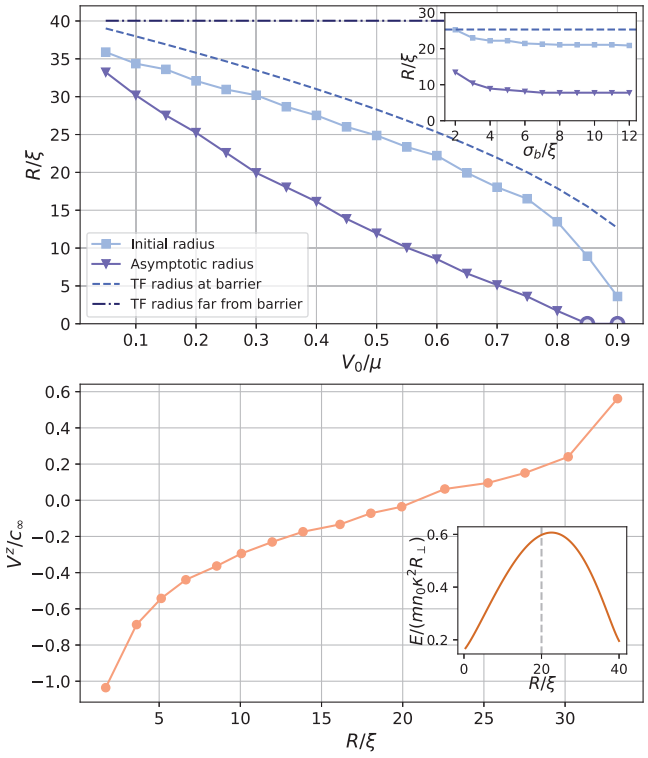

FIG. 3. Top panel: Initial (light-blue squares) and asymptotic (lilac triangles) vortex ring radii R at critical barrier velocity as a function of the barrier intensity V_0/μ with fixed $\sigma_b = 5\xi$. Inset: R as a function of barrier width σ_b with fixed $V_0 = 0.6\,\mu$. Open lilac circles indicate asymptotic radii set to zero as the rings self-annihilate before reaching an asymptotic regime. Bottom panel: Asymptotic vortex ring axial velocity V^z as a function of its asymptotic radius R reported in the top panel. Inset: Kinetic energy E of a cylindrical condensate in the presence of a vortex ring as a function of the ring's radius R; the dashed gray line at $R = 0.5R_{\perp\infty}$ marks where the slope would change sign in a homogeneous system. Here, n_0 indicates the particle number density on the cylinder axis.

is observed in both classical and quantum confined fluids [66,69,70], while the asymmetric characteristic emerging in Fig. 3 (bottom) is peculiar to BECs and arises from their compressibility and from the density modulation that can be achieved employing external potentials (for instance, in a classical homogeneous two-dimensional channel, the velocity is reversed exactly at $R/R_\perp = 0.5$ [50]). The velocity dependence on R and in particular the value of R for which vortex $V^z = 0$ can be determined, recalling that, as in classical fluid dynamics, quantum vortex rings and pairs follow Hamiltonian mechanics in both homogeneous [48] and inhomogeneous condensates [69,70]. Thus, the velocity of vortex rings is given by the following group-velocity relation:

$$V^z = \frac{\partial E}{\partial p_z} = \frac{\partial E/\partial R}{\partial p_z/\partial R}\,, \tag{2}$$

where $E = \int \frac{1}{2}\rho v^2 d\mathbf{x}$ is the kinetic energy induced by the vortex ring, $p_z = \int \rho v_z d\mathbf{x}$ is the momentum of the fluid in the axial direction, and v and v_z are the fluid velocity magnitude and its axial component, respectively. We compute analytically E and p_z in a cylindrical harmonic trap without the barrier and in the presence of a vortex ring, in order to study the asymptotic ring motion. In cylindrical coordinates, with no dependence on the azimuthal angle due to the symmetry of the problem, we approximate the condensate density $\rho(\mathbf{r})$ at a generic point $\mathbf{r} = (r, z)$ interpolating asymptotic forms of the density close and far away from the vortex located at $\mathbf{R} = (R, z_R)$ [71], R being the vortex ring radius and z_R its position along the cylinder axis. This yields $\rho \approx mn_0[\frac{|\mathbf{r}-\mathbf{R}|^2}{|\mathbf{r}-\mathbf{R}|^2+\xi^2}][1-(\frac{r_\perp}{R_\perp})^2]$, n_0 being the particle number density on the cylinder axis and $r_\perp$ distance from the latter. We employ a local velocity approximation according to which the velocity $\mathbf{v}$ of the fluid is only dictated by the closest vortex line element, namely, $\mathbf{v} = \boldsymbol{\kappa} \times (\mathbf{r} - \mathbf{R})/(2\pi|\mathbf{r} - \mathbf{R}|^2)$, where $\boldsymbol{\kappa}$ is the oriented vortex line element parallel to the vorticity with magnitude equal to the quantum of circulation $\kappa = h/m$ [50]. The behavior of E as a function of R is reported in Fig. 3 (bottom, inset) showing a slope sign switch for the same R where V^z changes its sign. Together with a monotonous behavior of $p_z(R)$ having a negative derivative for all R (see Appendix A), it explains the behavior of the vortex ring velocity. It is worth noting that the approximations employed in the analytical calculations are not able to describe reliably E and p_z for small radii.

To expand the variety of vortex interaction and generate excitations along the vortex rings, we include additional features in our platform. In particular, downstream with respect to the barrier, we shine two laser beams parallel to the y direction [Fig. 4 (top, left inset)], which correspond to local vertical potentials $V_i(\mathbf{x}) = V_c \exp\{-[(x - x_i)^2 + (z - z_c)^2]/2\sigma_c^2\}$, where $\sigma_c = 10\xi$, $V_c/\mu = 3/8$, $z_c = -10$, and $x_i = \pm 3$. The presence of these obstacles breaks the axial symmetry of the system and triggers the generation and propagation of almost planar Kelvin waves along the vortex rings [Fig. 4 (top)]. When the nucleated vortex rings approach the local potentials V_1 and V_2, between $t = 10$ and $t = 20$, $|z_R - z_c| < 3\sigma_c$ (z_R being the axial coordinate of the vortex ring), the size of BEC and its density are decreased by the potentials, resulting in an increase of the average vortex radius, as shown in Fig. 4 (bottom panel); this increase of the radius of the ring slows its motion, as reported in Fig. 4 (bottom panel), consistent with Fig. 3 (bottom). The expansion of the ring is not axially symmetric; the vortex increases its size in the x direction where the BEC is reduced by V_i, as shown from the evolution of the eccentricity e in Fig. 4 (top), where $e = \sqrt{1-(b/a)^2}$ if $a \geqslant b$ and $e = -\sqrt{1-(a/b)^2}$, a and b being the ellipse semiaxes in the x and y directions, respectively. The vortex ring hence becomes elliptical, corresponding to a Kelvin wave of mode $m = 2$, which then propagates [Fig. 4 (top, right inset)]. The oscillation frequency of the $m = 2$ Kelvin wave mode is consistent with previous analytical results [72]. Furthermore, by employing a single off-centered local vertical obstacle V_i, we intentionally break the linear propagation of the vortex ring and trigger an instability that drives it to crash onto the condensate boundary, highlighting the versatility of our 3D vortex-manipulation protocol (see Appendix C).

Conclusions. In conclusion, we present a protocol for the deterministic and reproducible generation of vortex rings in Bose–Einstein condensates that is experimentally realizable. By translating a planar optical sheet, our procedure directly

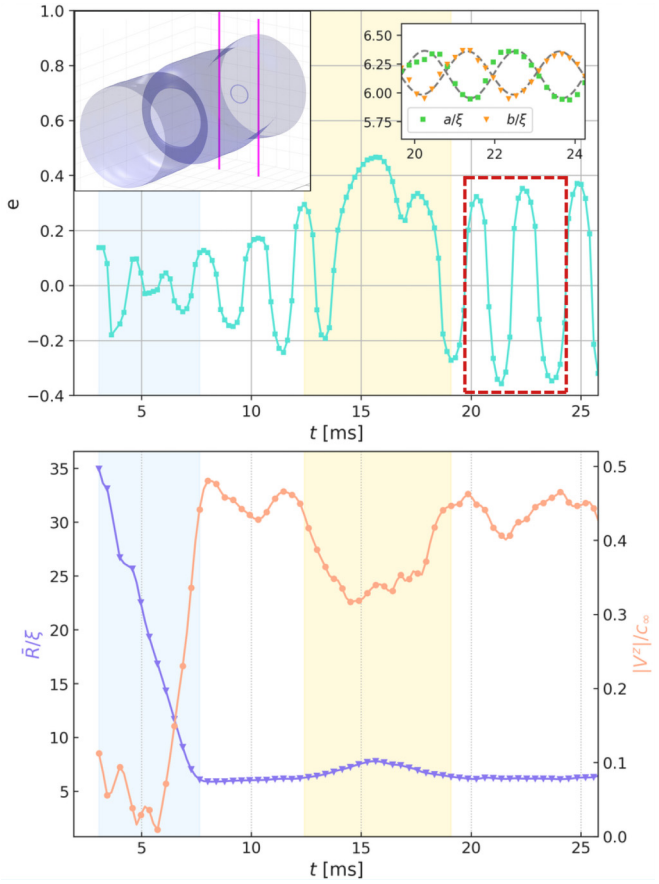

FIG. 4. Triggering of $m = 2$ Kelvin waves on a vortex ring. Top panel: Time evolution of the eccentricity of the vortex ring projection on the x–y plane. Left inset: BEC density isosurface, with the two local vertical potentials $V_i(\mathbf{x})$ represented as pink columns. Right inset: When the ring approaches the obstacles, they break the symmetry and excite oscillations of its semiaxes a and b; the dashed gray curve is a sinusoidal fit that matches the theoretical frequency of the $m = 2$ Kelvin wave. Bottom panel: Time evolution of the mean radius $\bar{R} = (a + b)/2$ (left axis, lilac triangles) and the velocity V^z of the vortex ring (right axis, light-pink circles). The blue area represents the region where the vortex interacts with the moving barrier, while the yellow area represents the region where it is affected by the vertical obstacles.

controls the radius of the nucleated rings, and hence their velocity, and emission frequency, enabling interactions between successively emitted rings (e.g., leapfrogging [47,66]). In addition, we show that by employing additional localized laser beams, we are able to change the shape, the radius, and the velocity of the ring, and to generate Kelvin waves on the ring itself. This comprehensive control of the generation and manipulation of vortex rings in experimentally achievable conditions could be highly relevant for the reproducible experimental study of quantum vortex-vortex interactions (including reconnections [29]), and the interplay between quantum vortices and boundaries (highly nontrivial with respect to the classical incompressible counterpart), and for the direct observation and investigation of quantum vortex-line excitations such as Kelvin waves without the use of particle tracers [73–75] trapped on vortices. The results we present may have an impact beyond quantum fluids, regarding fluid dynamics in general. Similarities between classical and quantum turbulence have suggested that turbulent flows, both classical and quantum, may be depicted on the basis of collective and interactive dynamics of thin vortex filaments of fixed circulation [37,38]: The study of quantum vortex interactions could thus lead to the enhancement of the understanding of the still open issues in classical turbulence.

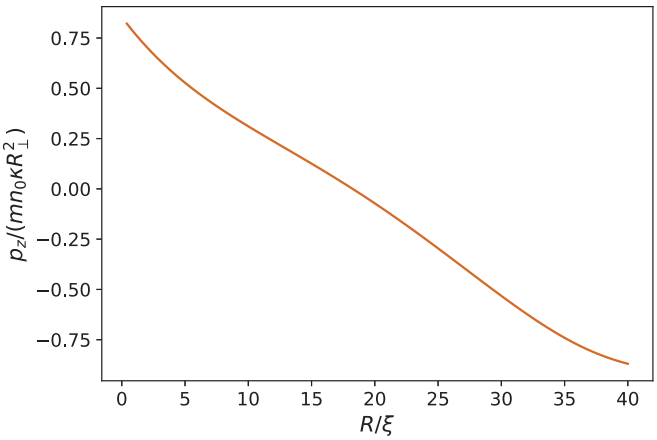

FIG. 5. Axial momentum p_z of a cylindrical condensate in the presence of a vortex ring as a function of the ring's radius R.

Acknowledgments. L.G. acknowledges fruitful discussions with Carlo Barenghi and Giovanni Franzina. D.E.G. and G.I. acknowledge fruitful discussions with Christian Apostoli. We acknowledge computational resources provided by INDACO Platform, which is a project of high performance computing at Università degli Studi di Milano. This work was supported by the European Research Council (ERC) under Grant Agreement No. 101076129 and the National Research Foundation of Korea (NRF) grant funded by the Korea government (MSIT) (RS-2024-00348882).

Data availability. The data that support the findings of this article are not publicly available upon publication because it is not technically feasible and/or the cost of preparing, depositing, and hosting the data would be prohibitive within the terms of this research project. The data are available from the authors upon reasonable request.

Appendix A: Momentum of vortex ring. The axial momentum of the BEC is defined as

$$p_z = \frac{1}{2i}\int\left(\Psi^*\frac{\partial\Psi}{\partial z} - \Psi\frac{\partial\Psi^*}{\partial z}\right)d\mathbf{r}\,. \tag{A1}$$

If we use the hydrodynamical formulation where $\Psi = \sqrt{n}e^{i\phi}$, where $n = \rho/m$ is the particle density number and ϕ is the phase such that the velocity $\mathbf{v} = \nabla\theta$, then

$$p_z = \int \rho(\mathbf{r})v_z(\mathbf{r})d\mathbf{r}\,, \tag{A2}$$

where v_z is the axial velocity of the fluid induced by the vortex ring. We compute analytically the integral as a function of the radius R of the vortex ring [50] and obtain the result reported in Fig. 5, where we observe that p_z is a decreasing function of R in the whole range. Hence, the velocity of the vortex ring reverses its sign when $\partial E/\partial R = 0$, i.e., for $R \sim 23\xi$.

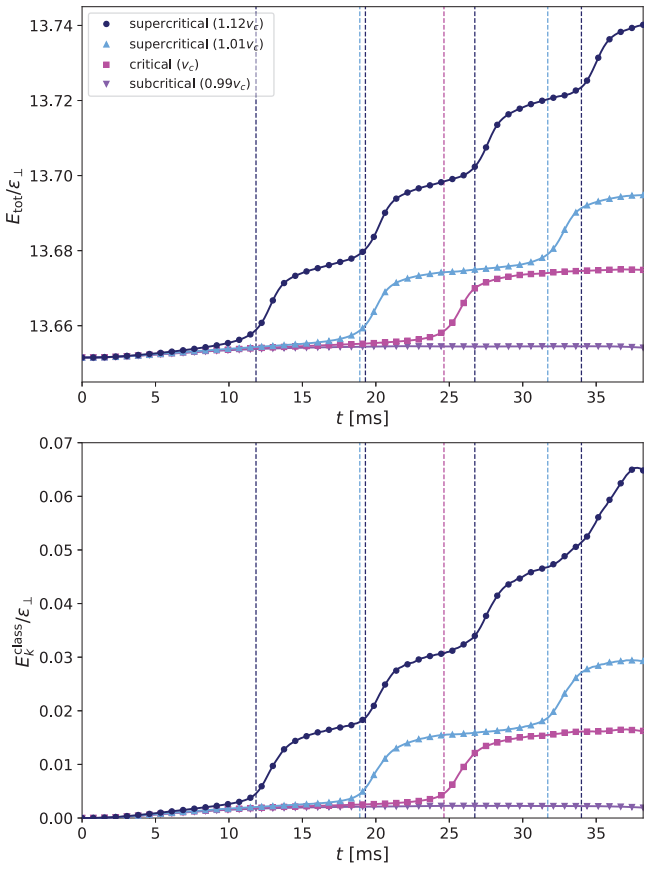

FIG. 6. Energy analysis during time evolution, for $V_0/\mu = 0.6$ and $\sigma_b = 2\xi$. Comparison between the critical case (barrier velocity $v_b^{\max} = v_c$, pink squares), a subcritical case ($v_b^{\max} = 0.99v_c$, lilac triangles), and two supercritical cases ($v_b^{\max} = 1.01v_c$, light-blue triangles, and $v_b^{\max} = 1.12v_c$, dark-blue circles). Top panel: Total energy $E_{\rm tot}$ of the superfluid, computed as the sum of kinetic, potential, and interaction energy contributions. Bottom panel: Temporal evolution of the classical kinetic energy $E_k^{\rm class}$. Vertical dashed lines mark the time instants when vortex rings are nucleated.

Appendix B: Energy analysis. The total energy of the system is given by the Gross-Pitaevskii energy functional

$$E_{\rm tot} = \int_\Omega d\Omega \left[\frac{1}{2}|\nabla\Psi|^2 + V|\Psi|^2 + \frac{g}{2}|\Psi|^4 \right], \qquad \text{(B1)}$$

where Ω denotes the computational domain corresponding to the numerical grid used to represent the system. By analyzing the time evolution of the total energy and its individual contributions, we observe that at the beginning the total energy increases monotonically in time, reflecting the continuous energy injection induced by the hyperbolic-tangent ramp-up of the barrier velocity. Most interestingly, while no remarkable energetic features are observed in the subcritical regime, for $v_b^{max} \geqslant v_c$ each vortex nucleation event is associated with a change in the slope of the total energy $E_{\rm tot}$ and the classical kinetic energy $E_k^{\rm class} = \int_\Omega d\Omega \frac{1}{2}\rho v^2$ [Fig. 6 (top) and (bottom), respectively], followed by a sharper increase and a subsequent quasiplateau. When a vortex is nucleated and leaves the low-density region created by the barrier traveling toward the bulk, it increases the kinetic energy (and hence the total energy) of the BEC as the density surrounding the vortex ring is larger. This increase continues until the vortex reaches its asymptotic propagation regime in the bulk. Thereon, the total energy exhibits a quasiplateau until a new vortex nucleation event occurs, producing a further increase.

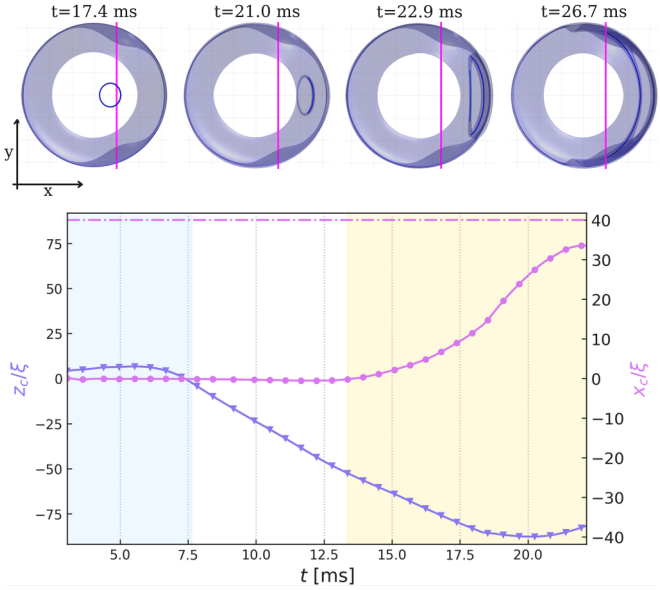

FIG. 7. Triggering of vortex ring destabilization. Top panel: BEC density isosurfaces at four different times viewed frontally along the z axis; the local vertical potential $V(\mathbf{x})$ is represented as a pink column. Bottom panel: Time evolution of the vortex center's x (pink circles) and z (blue triangles) positions. After leaving the blue area—where the vortex interacts with the moving barrier—the vortex exhibits its usual linear motion along the z axis, with no motion in the x direction. Upon entering the pink area—where density is strongly affected by the vertical obstacle—the vortex center's x coordinate starts increasing linearly, showing that the vortex is bending toward the obstacle. Eventually, the x velocity increases, while the z velocity decreases, until the vortex approaches the trap boundary. The dash-dot line indicates the trap Thomas-Fermi radius.

Appendix C: Destabilization of vortex ring. In order to trigger the destabilization of the vortex ring, we employ one of the laser beams used for the excitation of Kelvin waves in Fig. 4, but position it off center. The local vertical potential representing the laser beam is thus $V(\mathbf{x}) = V_c \exp\{-[(x-x_c)^2 + (z-z_c)^2]/2\sigma_c^2\}$, where $\sigma_c = 10\xi$, $V_c/\mu = 3/8$, and $z_c = -10$ as in the previous case, while $x_c = 2$. The vortex ring reaches the region where the density is significantly affected by the local potential at $t \approx 13.5$ ms (yellow area in Fig. 7, top). From that time onward, the ring starts bending toward the beam until crashing onto the boundary. This behavior is shown in Fig. 7 both visually (top) and by noting that after $t \approx 13.5$ ms the vortex acquires a linear motion in the positive x direction, while its motion along the z axis of the cylinder is eventually suppressed, leading to its final impact with the boundary (bottom). We observe that the strong density depletion at the boundary leads to a substantial enlargement of the vortex as it approaches the edge.

[1] I. Chuang, R. Durrer, N. Turok, and B. Yurke, Cosmology in the laboratory: Defect dynamics in liquid crystals, Science **251**, 1336 (1991).

[2] E. Priest and T. Forbes, *Magnetic Reconnection: MHD Theory and Applications* (Cambridge University Press, Cambridge, 2007).

[3] H. Che, J. Drake, and M. Swisdak, A current filamentation mechanism for breaking magnetic field lines during reconnection, Nature (London) **474**, 184 (2011).

[4] J. W. Cirtain, L. Golub, A. Winebarger, B. De Pontieu, K. Kobayashi, R. Moore, R. W. Walsh, K. Korreck, M. Weber, P. McCauley, *et al.*, Energy release in the solar corona from spatially resolved magnetic braids, Nature (London) **493**, 501 (2013).

[5] M. Dennis, R. King, B. Jack, K. O'Holleran, and M. Padgett, Isolated optical vortex knots, Nat. Phys. **6**, 118 (2010).

[6] M. Berry and M. Dennis, Reconnections of wave vortex lines, Eur. J. Phys. **33**, 723 (2012).

[7] M. Farge, G. Pellegrino, and K. Schneider, Coherent vortex extraction in 3D turbulent flows using orthogonal wavelets, Phys. Rev. Lett. **87**, 054501 (2001).

[8] I. Marusic and J. P. Monty, Attached eddy model of wall turbulence, Annu. Rev. Fluid Mech. **51**, 49 (2019).

[9] R. J. Donnelly, *Quantized Vortices in Helium II* (Cambridge University Press, Cambridge, 1991).

[10] C. Barenghi, R. Donnelly, and W. Vinen, *Quantized Vortex Dynamics and Superfluid Turbulence* (Springer, Heidelberg, 2001).

[11] C. F. Barenghi, L. Skrbek, and K. R. Sreenivasan, *Quantum Turbulence* (Cambridge University Press, Cambridge, 2023).

[12] L. F. Richardson, *Weather Prediction by Numerical Process* (Cambridge University Press, Cambridge, 1922).

[13] A. Kolmogorov, The local structure of turbulence in an incompressible viscous fluid for very large Reynolds numbers, Dokl. Akad. Nauk. SSSR **30**, 301 (1941).

[14] J. Maurer and P. Tabeling, Local investigation of superfluid turbulence, Europhys. Lett. **43**, 29 (1998).

[15] C. Barenghi, V. L'vov, and P. Roche, Experimental, numerical and analytical velocity spectra in turbulent quantum fluid, Proc. Natl. Acad. Sci. USA **111**, 4683 (2014).

[16] A. W. Baggaley, C. F. Barenghi, A. Shukurov, and Y. A. Sergeev, Coherent vortex structures in quantum turbulence, Europhys. Lett. **98**, 26002 (2012).

[17] C. Nore, M. Abid, and M. E. Brachet, Kolmogorov turbulence in low-temperature superflows, Phys. Rev. Lett. **78**, 3896 (1997).

[18] L. Galantucci, E. Rickinson, A. W. Baggaley, N. G. Parker, and C. F. Barenghi, Dissipation anomaly in a turbulent quantum fluid, Phys. Rev. Fluids **8**, 034605 (2023).

[19] W. F. Vinen, Decay of superfluid turbulence at a very low temperature: The radiation of sound from a Kelvin wave on a quantized vortex, Phys. Rev. B **64**, 134520 (2001).

[20] D. Kivotides, J. C. Vassilicos, D. C. Samuels, and C. F. Barenghi, Kelvin waves cascade in superfluid turbulence, Phys. Rev. Lett. **86**, 3080 (2001).

[21] V. L'vov and S. Nazarenko, Spectrum of Kelvin-wave turbulence in superfluids, JETP Lett. **91**, 428 (2010).

[22] E. Kozik and B. Svistunov, Kelvin-wave cascade and decay of superfluid turbulence, Phys. Rev. Lett. **92**, 035301 (2004).

[23] A. C. White, B. P. Anderson, and V. S. Bagnato, Vortices and turbulence in trapped atomic condensates, Proc. Natl. Acad. Sci. USA **111**, 4719 (2014).

[24] R. Panico, P. Comaron, M. Matuszewski, A. Lanotte, D. Trypogeorgos, G. Gigli, M. De Giorgi, V. Ardizzone, D. Sanvitto, and D. Ballarin, Onset of vortex clustering and inverse energy cascade in dissipative quantum fluids, Nat. Photon. **17**, 451 (2023).

[25] B. Haskell and A. Melatos, Models of pulsar glitches, Int. J. Mod. Phys. D **24**, 1530008 (2015).

[26] L. Onsager, Statistical hydrodynamics, Nuovo Cim. **6**, 279 (1949).

[27] R. P. Feynman, Application of quantum mechanics to liquid helium, in *Progress in Low Temperature Physics*, edited by C. J. Gorter (Elsevier, New York, 1955), Chap. II.

[28] W. Vinen, The detection of single quanta of circulation in liquid helium II, Proc. R. Soc. Lond. A **260**, 218 (1961).

[29] S. Serafini, L. Galantucci, E. Iseni, T. Bienaime, R. N. Bisset, C. F. Barenghi, F. Dalfovo, G. Lamporesi, and G. Ferrari, Vortex reconnections and rebounds in trapped atomic Bose-Einstein condensates, Phys. Rev. X **7**, 021031 (2017).

[30] L. Galantucci, A. W. Baggaley, N. G. Parker, and C. F. Barenghi, Crossover from interaction to driven regimes in quantum vortex reconnections, Proc. Natl. Acad. Sci. USA **116**, 12204 (2019).

[31] A. Villois, D. Proment, and G. Krstulovic, Irreversible dynamics of vortex reconnections in quantum fluids, Phys. Rev. Lett. **125**, 164501 (2020).

[32] G. W. Stagg, N. G. Parker, and C. F. Barenghi, Superfluid boundary layer, Phys. Rev. Lett. **118**, 135301 (2017).

[33] G. Krstulovic and M. E. Brachet, Kelvin waves, mutual friction, and fluctuations in the Gross–Pitaevskii model, J. Low Temp. Phys. **212**, 321 (2023).

[34] S. R. Stalp, L. Skrbek, and R. J. Donnelly, Decay of grid turbulence in a finite channel, Phys. Rev. Lett. **82**, 4831 (1999).

[35] M. La Mantia and L. Skrbek, Quantum, or classical turbulence? Europhys. Lett. **105**, 46002 (2014).

[36] N. P. Müller, J. I. Polanco, and G. Krstulovic, Intermittency of velocity circulation in quantum turbulence, Phys. Rev. X **11**, 011053 (2021).

[37] J. I. Polanco, N. P. Müller, and G. Krstulovic, Vortex clustering, polarisation and circulation intermittency in classical and quantum turbulence, Nat. Commun. **12**, 7090 (2021).

[38] L. Galantucci, Quantum turbulent flows: A model for classical turbulence? J. Fluid Mech. **1022**, F1 (2025).

[39] E. C. Samson, K. E. Wilson, Z. L. Newman, and B. P. Anderson, Deterministic creation, pinning, and manipulation of quantized vortices in a Bose-Einstein condensate, Phys. Rev. A **93**, 023603 (2016).

[40] W. Kwon, G. Del Pace, K. Xhani, L. Galantucci, A. Muzi Falconi, M. Inguscio, F. Scazza, and G. Roati, Sound emission and annihilations in a programmable quantum vortex collider, Nature (London) **600**, 64 (2021).

[41] S. Serafini, M. Barbiero, M. Debortoli, S. Donadello, F. Larcher, F. Dalfovo, G. Lamporesi, and G. Ferrari, Dynamics and interaction of vortex lines in an elongated Bose-Einstein condensate, Phys. Rev. Lett. **115**, 170402 (2015).

[42] A. Burchianti, F. Scazza, A. Amico, G. Valtolina, J. A. Seman, C. Fort, M. Zaccanti, M. Inguscio, and G. Roati,

Connecting dissipation and phase slips in a Josephson junction between fermionic superfluids, Phys. Rev. Lett. **120**, 025302 (2018).
[43] M. E. Mossman, M. A. Hoefer, K. Julien, P. Kevrekidis, and P. Engels, Dissipative shock waves generated by a quantum-mechanical piston, Nat. Commun. **9**, 4665 (2018).
[44] F. Piazza, L. A. Collins, and A. Smerzi, Instability and vortex ring dynamics in a three-dimensional superfluid flow through a constriction, New J. Phys. **13**, 043008 (2011).
[45] K. Xhani, E. Neri, L. Galantucci, F. Scazza, A. Burchianti, K. L. Lee, C. F. Barenghi, A. Trombettoni, M. Inguscio, M. Zaccanti, G. Roati, and N. P. Proukakis, Critical transport and vortex dynamics in a thin atomic Josephson junction, Phys. Rev. Lett. **124**, 045301 (2020).
[46] K. Xhani, L. Galantucci, C. F. Barenghi, G. Roati, A. Trombettoni, and N. P. Proukakis, Dynamical phase diagram of ultracold Josephson junctions, New J. Phys. **22**, 123006 (2020).
[47] V. Singh, L. Mathey, H. Ott, and L. Amico, Controlled generation of 3D vortices in driven atomic Josephson junctions, arXiv:2511.05645.
[48] C. A. Jones and P. H. Roberts, Motions in a Bose condensate. IV. Axisymmetric solitary waves, J. Phys. A: Math. Gen. **15**, 2599 (1982).
[49] L. P. Pitaevskii and S. Stringari, *Bose-Einstein Condensation* (Oxford University Press, Oxford, 2003).
[50] See Supplemental Material at http://link.aps.org/supplemental/10.1103/qvg7-mr18 for details on numerical simulations, system setup and technical implementation, which includes Refs. [51,52].
[51] G. Stagg, 2D-GP (2014), https://github.com/georgestagg/2D-GP.
[52] P. K. Newton, *The N-Vortex Problem: Analytical Techniques* (Springer, New York, 2001), Vol. 145.
[53] G. Iori, Simulation of 3D quantum vortex nucleation in trapped Bose-Einstein condensates, Master's thesis, Università degli Studi di Milano, Milan, Italy, 2025.
[54] N. Berloff and P. Roberts, Motions in a Bose condensate: VII. Boundary-layer separation, J. Phys. A: Math. Gen. **33**, 4025 (2000).
[55] G. Stagg, N. Parker, and C. Barenghi, Quantum analogues of classical wakes in Bose–Einstein condensates, J. Phys. B: At. Mol. Opt. Phys. **47**, 095304 (2014).
[56] W. J. Kwon, G. Moon, S. W. Seo, and Y. Shin, Critical velocity for vortex shedding in a Bose-Einstein condensate, Phys. Rev. A **91**, 053615 (2015).
[57] T. Frisch, Y. Pomeau, and S. Rica, Transition to dissipation in a model of superflow, Phys. Rev. Lett. **69**, 1644 (1992).
[58] S. Musser, D. Proment, M. Onorato, and W. T. M. Irvine, Starting flow past an airfoil and its acquired lift in a superfluid, Phys. Rev. Lett. **123**, 154502 (2019).
[59] T. Frisch, S. Nazarenko, and S. Rica, Superflow passing over a rough surface: Vortex nucleation, Phys. Rev. Fluids **9**, 024701 (2024).
[60] C. Huepe and M.-E. Brachet, Scaling laws for vortical nucleation solutions in a model of superflow, Physica D **140**, 126 (2000).
[61] C. Rorai, J. Skipper, R. Kerr, and K. Sreenivasan, Approach and separation of quantum vortices with balanced cores, J. Fluid Mech. **808**, 641 (2016).
[62] A. Villois, G. Krstulovic, and H. Proment, D. Salman, A vortex filament tracking method for the Gross-Pitaevskii equation, J. Phys. A: Math. Theor. **49**, 415502 (2016).
[63] K. Sasaki, N. Suzuki, and H. Saito, Bénard–von Kármán vortex street in a Bose-Einstein condensate, Phys. Rev. Lett. **104**, 150404 (2010).
[64] W. J. Kwon, J. H. Kim, S. W. Seo, and Y. Shin, Observation of von Kármán vortex street in an atomic superfluid gas, Phys. Rev. Lett. **117**, 245301 (2016).
[65] T. Aioi, T. Kadokura, T. Kishimoto, and H. Saito, Controlled generation and manipulation of vortex dipoles in a Bose-Einstein condensate, Phys. Rev. X **1**, 021003 (2011).
[66] L. Galantucci, M. Sciacca, N. G. Parker, A. W. Baggaley, and C. F. Barenghi, Classical and quantum vortex leapfrogging in two-dimensional channels, J. Fluid Mech. **912**, A9 (2021).
[67] P. H. Roberts and J. Grant, Motions in a Bose condensate. I. The structure of the large circular vortex, J. Phys. A: Gen. Phys. **4**, 55 (1971).
[68] P. Mason, N. G. Berloff, and A. L. Fetter, Motion of a vortex line near the boundary of a semi-infinite uniform condensate, Phys. Rev. A **74**, 043611 (2006).
[69] P. Mason and N. G. Berloff, Motion of quantum vortices on inhomogeneous backgrounds, Phys. Rev. A **77**, 032107 (2008).
[70] S. Komineas and N. Papanicolaou, Vortex rings and Lieb modes in a cylindrical Bose-Einstein condensate, Phys. Rev. Lett. **89**, 070402 (2002).
[71] B. Jackson, J. F. McCann, and C. S. Adams, Vortex line and ring dynamics in a trapped Bose-Einstein condensate, Phys. Rev. A **61**, 013604 (1999).
[72] H. Pocklington, The complete system of the periods of a hollow vortex ring, Philos. Trans. R. Soc. Lond., Ser. A **186**, 603 (1895).
[73] E. Fonda, D. Meichle, N. Ouellette, S. Hormoz, and D. Lathrop, Direct observation of Kelvin waves excited by quantized vortex reconnection, Proc. Natl. Acad. Sci. USA **111**, 4707 (2014).
[74] C. Peretti, J. Vessaire, É. Durozoy, and M. Gibert, Direct visualization of the quantum vortex lattice structure, oscillations, and destabilization in rotating ^{4}He, Sci. Adv. **9**, eadh2899 (2023).
[75] Y. Minowa, Y. Yasui, T. Nakagawa, S. Inui, M. Tsubota, and M. Ashida, Direct excitation of Kelvin waves on quantized vortices, Nat. Phys. **21**, 233 (2025).